Hindawi
Advances in Civil Engineering
Volume 2023, Article ID 8090935, 10 pages
https://doi.org/10.1155/2023/8090935

Research Article

Experimental Investigation on the Influence of Water Injection Timing on the Deformation of Loose Rock Blocks

Baoliang Zhang,[1] Jian Li,[1] Yongqiang Zhou,[2] Yi Geng,[1] Qingshuang Zhao,[1] Dezhi Kong,[3] Zihao Zhao,[4] and Changxiang Wang[2]

[1]*School of Architecture and Civil Engineering, Liaocheng University, Liaocheng 252000, China*
[2]*State Key Laboratory of Mining Response and Disaster Prevention and Control in Deep Coal Mines, Anhui University of Science and Technology, Huainan, Anhui 232001, China*
[3]*Student Affairs Office, Wenzhou Medical University, Wenzhou 325000, China*
[4]*Jining No.2 Coal Mine, Yanzhou Coal Mining Co., Ltd, Jining 272000, China*

Correspondence should be addressed to Changxiang Wang; 1554624100@qq.com

Received 11 April 2023; Revised 11 June 2023; Accepted 3 July 2023; Published 25 July 2023

Academic Editor: Andrea Pranno

This study investigated the influence of water injection timing on the compression deformation of loose rock blocks in the goaf. The study used a confined gradient loading compression test to examine the deformation of loose rock blocks under initial saturation and later immersion conditions. The results showed that under initial saturation, the deformation of each loading gradient and the whole loading stage was greater than that of the later immersion stage. Additionally, the deformation of different stages in the initial saturated state was relatively regular, while in the later immersion state, the deformation changed abruptly after immersion. To explain the deformation mechanism of loose rock blocks, the mesostructure of loose rock blocks was granulated and the contact mechanism of particles was studied. The study found that water weakens the effective contact stress and strength between the skeleton particles, leading to sliding deformation as the dominant deformation mode. The study provides a theoretical basis for understanding the deformation characteristics of loose rock blocks in the goaf under different water environments.

1. Introduction

After coal seams are mined, the overlying strata undergo a series of bending, subsidence, rupture, and movement damage due to gravity and upper load. One popular green mining method to control roof subsidence, avoid uncontrollable damage, and eliminate the underground lifting and ground storage of gangue is gangue filling mining [1–5]. Figure 1 shows the gangue filling effect. The deformation behavior of loose rock blocks is closely linked to the effects of self-weight and the overlying rock load. These factors have a direct impact on the development characteristics of fractures in the overlying rock, as well as on the overall surface stability over the goaf [6, 7]. The evaluation of deformation characteristics of loose rock blocks in a goaf is a challenging task, owing to inherent limitations in the test equipment and conditions. In order to overcome these challenges, it is often necessary to downscale the gravel rock mass, which may result in variations in the particle size distribution of the gangue sample tested vis-à-vis the natural gangue. These disparities, compounded by potential inaccuracies in human and equipment factors, can lead to errors in the site evaluation, thereby impairing the overall reliability of the test results [8, 9]. Despite the inherent limitations associated with simulation testing, it is worth noting that the results obtained from such tests can provide a fundamental understanding of the engineering properties of loose rock blocks in a goaf. Such insights are critical for comprehending the physical and mechanical properties of these blocks under different conditions. Therefore, while acknowledging the potential for disparities due to scaling, simulation testing remains a valuable tool for obtaining a basic understanding of the behavior of loose rock blocks in goafs.

The bearing pressure of loose rock blocks in goaf is related to the fracture of main roof rock beam [10]. Between two successive roof weightings, the pressure acting on the

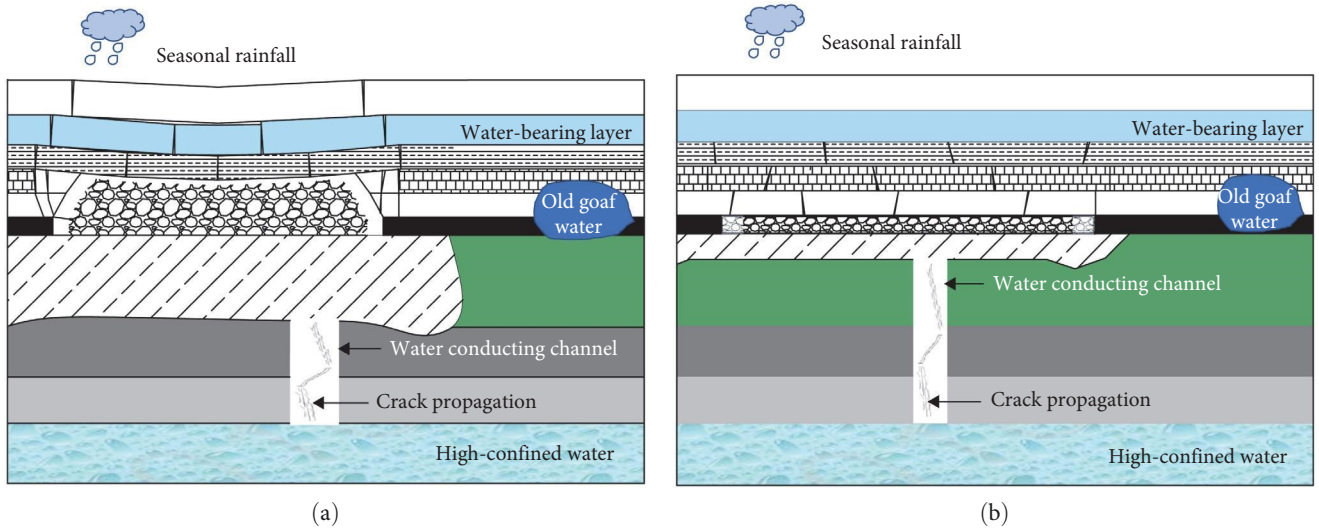

Figure 1: The gangue filling effect and the different water sources on the loose rock blocks: (a) traditional fully mechanized mining and (b) filling fully mechanized mining.

caving rock is relatively constant and comparable to the self-weight stress of the overlying fractured rock layer. However, during the roof weighting process, the pressure exerted on the caving rock sharply increases and is proportional to the self-weight stress of the newly fractured rock stratum in the overlying strata. This phenomenon highlights the significant impact of roof weightings on the stress distribution and deformation behavior of the caving rock in underground mining operations. The stress state of the loose rock blocks does not increase linearly, but gradually increases in a stepwise manner with the continuous advancement of the working face [11, 12]. Therefore, the grading loading mode is more effective in simulating the stress and deformation characteristics of filling gangue in a real goaf.

Under certain geological conditions or climatic conditions, the loose rock blocks may be immersed in water, which greatly changes their mechanical properties. Figure 1 shows the influence of groundwater level rise, aquifer leakage, seasonal rainfall, and goaf water filling on loose rock blocks. Li et al. [13] analyzed the deformation and crushing characteristics of loose rock blocks under different immersion heights by using confined compression experiments. The results showed that the crushing rate and maximum axial strain of loose rock blocks gradually increased with the immersion height. Lu et al. [14] studied the different distribution patterns of energy dissipation in natural state and water-bearing state. Ma et al. [15, 16] studied the deformation characteristics of saturated broken coal, shale, and sandstone, and further studied the variation law of pores in mudstone creep process by using self-made broken rock mass test device. Chen et al. [17] studied the influence of saturated water on the compaction characteristics of coal seam roof gravel by using a self-made device. The results show that the effect of water on different strength gravel is different, the effect on low-strength mudstone is stronger, and the effect on high-strength sandstone is weaker. The effect of water on the compaction of small-diameter gravel is greater than that of large-diameter gravel.

At present, the research on the compaction characteristics of loose rock blocks is basically a single water content state, and the influence of different water content states on the deformation of loose rock blocks is less studied. Due to the limitation of test equipment, the diameter height ratio of general test bin is small, the corresponding loose rock blocks particle size is small, the size effect is more obvious. The author's team developed a large-scale loose rock blocks deformation-seepage experimental system in order to obtain data closer to the coal mine site.

The author's team has published a paper used this experimental equipment [18]. Because the experimental equipment used is the same, there are some similarities. However, the process of experimental analysis of these two papers is different. The published paper carried out a set of experiments to analyze the effect of gradient loading and water on the deformation of loose rock blocks. In this paper, two sets of comparative experiments were carried out to analyze the influence of water injection time on deformation. Considering the complex environment of loose rock blocks in goaf, two test processes of initial saturation and later immersion were designed to reveal the role of water content in the bearing and deformation process of loose rock blocks, so as to provide targeted basic data for surface subsidence prediction for filling mining coal mines under different water environments, and to do a good job in the protection of corresponding surface buildings and groundwater.

2. Test Method

2.1. Test Equipment

2.1.1. Control System. The experimental control system comprises of two main components: the console and the servo loading system. The servo loading system, in turn, is comprised of two distinct subsystems: the water pressure and water double control servo system, as well as the displacement stress double control servo system. Together, these components enable computerized automatic control over

Figure 2: Testing control system.

Table 1: Parameters of experimental system.

Axial compression	≤600 kN	Axial compression accuracy	0.01 kN
Water hydraulic	≤2 MPa	Water hydraulic accuracy	0.01 MPa
Hydraulic cylinder displacement	≤500 mm	Displacement accuracy	0.01 mm
Experimental box diameter	400 mm	Experimental box height	680 mm

the entire experimental process. The graphical representation of the experimental control system is illustrated in Figure 2.

2.1.2. Loading and Unloading System. The experimental system is shown in Figure 2, and the main parameters are shown in Table 1.

2.2. Test Principle. During the mining process, the environment of water is redistributed, water can play the role of lubricant, and the friction coefficient between broken rocks is reduced, so that the strength of broken rocks is reduced. Water can significantly impact rock mass through two primary mechanisms. The first mechanism is the mechanical effect of water on rock mass, which is primarily characterized by the hydrostatic pressure-induced effective stress and the erosion effect of hydrodynamic pressure. The second mechanism involves the physical and chemical action of water on rock mass, which can result in the softening, mudification, and dissolution of the rock mass. These processes gradually deteriorate the properties of the rock mass, leading to its deformation, instability, and ultimate failure.

First of all, the mechanism of water softening effect on rock mass, different rocks contain different mineral composition, so it also determines the nature of its softening and expansion in contact with water, most of the rock mass contains clay minerals, these minerals soften mud in contact with water, reduces the bonding force of the rock mass skeleton, thus showing the softening properties of all aspects. The quantitative expression of the softening effect of water on rock mass is generally expressed by Young's modulus, compressive resistance, shear strength, and other parameters. The moisture content, uniaxial compressive strength, and Young's modulus have the following empirical formulas:

Effect of moisture content W_c on uniaxial strength of rock σ_c is given as follows:

$$\sigma_c = a - bW_c. \tag{1}$$

Effect of moisture content W_c on Young's modulus E is given as follows:

$$E = \frac{a}{W_c} - b. \tag{2}$$

Effect of pore water pressure p on Young's modulus E is given as follows:

$$E = a - bp. \tag{3}$$

In this paper, two sets of experiments are designed to analyze the influence of water filling time on the deformation of gangue filling in goaf area, that is, initial invasion and late invasion.

3. Initial Saturated Gradient Loading Experiment

3.1. Experimental Scheme. A self-made large-size loose rock blocks deformation–seepage experimental system were used to conduct compaction test on loose rock blocks. The deformation characteristics of broken roof rock during compaction are analyzed below.

(1) The rock samples selected for testing primarily consist of sandstone, limestone, and mudstone. The samples are weighed and measured for volume before being broken into smaller rock blocks with a maximum particle size of 60 mm. These smaller blocks are then sorted into four size grades, 0–15, 15–30, 30–45, and 45–60 mm, using sieves with apertures of 15, 30, 45, and 60 mm, respectively.

(2) The loose rock blocks, categorized by size and lithology, are mixed together and loaded into a test barrel with a diameter of 400 mm and a height of 600 mm.

(3) During the loading stage, the axial load is incremented in steps of 100 kN, starting from 100 kN and ending at 500 kN. The loading rate is 0.5 kN/s, and the axial load of each stage is maintained for 0.5 hr to avoid prolonged pump pressurization. The axial load is gradually increased at each stage until the test is completed.

(4) According to the data results obtained from the above steps, the change of loose rock blocks with load gradient is analyzed, and the compaction deformation stage and displacement–load function curve are obtained.

3.2. Experimental Results. In preparation for the compaction test, the loose rock blocks were subjected to a saturation process by immersion in water for five hours. A water pressure of 0.2 MPa was applied to the system during the test. The loading process was monitored and recorded, and the resulting time–load and time–displacement curves are presented in Figures 3 and 4, respectively. The deformation parameters obtained from the test are summarized in Table 2.

Table 2 and Figure 3 illustrate that the displacement increments during the initial saturated loading stage, specifically 39.86, 29.13, 19.36, 7.41, and 4.97 mm, exhibit a gradual reduction. In the subsequent dead load stage, the displacement increments for each level are 6.47, 8.36, 12.43, 4.83, and 3.39 mm, respectively. The cumulative displacement for the loose rock blocks compaction test is 136.21 mm, of which 100.73 mm corresponds to the loading displacement increment, accounting for 73.95% of the total displacement, and 35.48 mm corresponds to the dead load displacement increment, accounting for 26.05% of the total displacement.

Based on Table 2 and Figure 3, it is observed that the displacement curve during the initial water-saturated loading stage exhibits significant large-step growth, primarily resulting from the stepwise increase in loading load. The axial

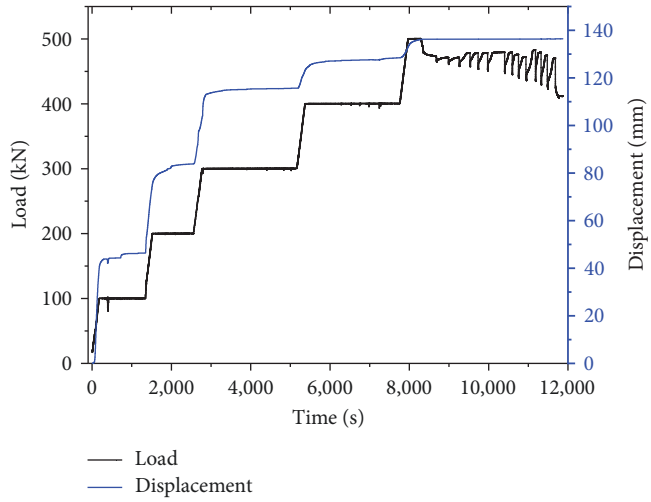

Figure 3: Load and deformation over time of initial saturated loading experiment.

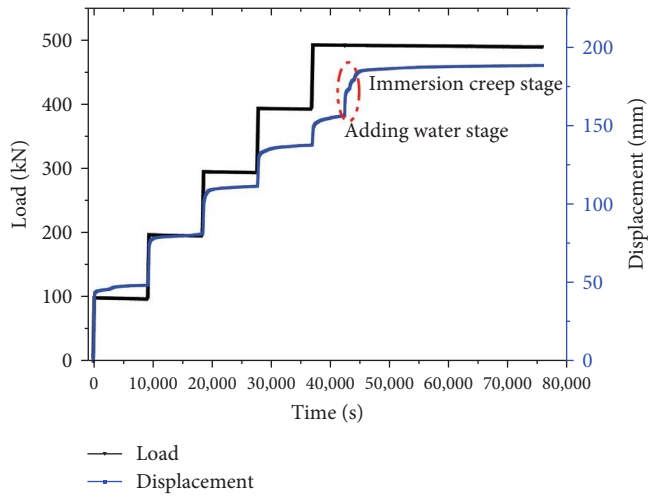

Figure 4: Load and deformation over time of later immersion gradient loading experiment.

displacement of each graded dead load stage under saturated water conditions shows a gradual increase. During the 100 kN dead load stage, there are three notable small-step displacement increases, with the maximum step displacement increase approaching 2 mm. Additionally, a special phenomenon of displacement rebound is observed, indicating significant changes in the loose rock block structure under the influence of water. In the goaf containing water, the loose rock blocks tend to be more closely compacted, which may result in an increase in the subsidence value of the overlying strata due to the softening effect of water.

4. Postimmersion Gradient Loading Experiment

4.1. Experimental Scheme. Underground broken rock has stratification, partition, that is, within a certain space broken rock particle size difference is not large, rather than a

Table 2: Deformation parameters in initial saturated state.

Test stage	Deformation			
	Initial (mm)	End (mm)	Difference (mm)	Deformation
0–100 kN loading	0	39.86	39.86	0.0699
100 kN dead load	39.86	46.33	6.47	0.0114
100–200 kN loading	46.33	75.46	29.13	0.0511
200 kN dead load	75.46	83.82	8.36	0.0147
200–300 kN loading	83.82	103.18	19.36	0.0340
300 kN dead load	103.18	115.61	12.43	0.0218
300–400 kN loading	115.61	123.02	7.41	0.0130
400 kN dead load	123.02	127.85	4.83	0.0085
400–500 kN loading	127.85	132.82	4.97	0.0087
500 kN dead load	132.82	136.21	3.39	0.0059

Table 3: Deformation parameters in postimmersion state.

Test stage	Deformation			
	Initial (mm)	End (mm)	Difference (mm)	Deformation (10^{-3})
0–100 kN loading	0	41.77	41.77	65.940
100 kN dead load	41.77	48.7	6.93	10.940
100–200 kN loading	48.7	72.18	23.48	37.066
200 kN dead load	72.18	81.21	9.03	14.255
200–300 kN loading	81.21	99.58	18.37	28.999
300 kN dead load	99.58	111.8	12.22	19.291
300–400 kN loading	111.8	125.1	13.22	20.869
400 kN dead load	125.1	137.9	12.93	20.411
400–500 kN loading	137.9	146.9	8.97	14.160
500 kN dead load	146.9	157.1	10.24	16.165
Watering stage	157.3	173.6	16.23	25.621
Soaking creep stage	173.6	189.0	15.46	24.405

continuous gradation distribution characteristics, but concentrated in a particle size range. Considering this, the particle size of the broken rock is designed to be in the range of 40–50 mm. The complete roof of the large pieces of red sandstone mashed, with a nominal diameter of 50 and 60 mm round hole sieve screening step by step.

In the experiment of compressive deformation of broken rock, trapezoidal step loading is designed. The axial load of each stage is 100, 200, 300, 400, 500 kN, and the loading gradient is 100 kN. The loading rate is 0.5 kN/s, 100, 200, 300, and 400 kN load gradient constant load time is 2.5 hr. Among them, the axial load is increased to 500 kN with a loading rate of 0.5 kN/s, and the axial load of 500 kN is maintained for 1.25 hr. After the five-stage active loading to 1.25 hr, water was injected into the cabin, and the broken rock was just soaked to carry out the creep experiment under the soaking state.

4.2. Experimental Results. Figure 4 and Table 3 illustrate the relationship between axial load and time, as well as the relationship between axial deformation and time during the later immersion gradient loading experiment. Notably, water significantly accelerates axial deformation, with the effect of graded loading gradient on axial deformation being less pronounced in this stage. In the initial stage of water injection, the axial deformation of loose rock blocks demonstrates a linearly increasing trend. As the water volume increases, the axial deformation of loose rock blocks continues to increase, albeit at a slower rate. Following the water injection stage, the axial deformation transitions to immersion creep deformation, with a gradual increase in deformation. The creep persisted for ~8 hr, resulting in a compression amount of 189.06 mm after the immersion creep experiment.

As shown in Table 3 and Figure 4, the displacement increments of each loading stage in later immersion are 41.77, 23.48, 18.37, 13.22, and 8.97 mm, respectively. The displacement increments of each load level in the later soaking stage were 6.93, 9.03, 12.22, 12.93, and 10.24 mm, respectively. The displacement increments in the later immersion and water-adding stage and the immersion constant load stage are 16.23 and 15.46 mm, respectively. Before adding water, the total displacement of loose rock blocks compaction test is 157.10 mm, loading displacement increment is 105.80 mm, dead load displacement increment is 51.30 mm, after adding water, the total displacement of loose rock blocks compaction test is 189.00 mm.

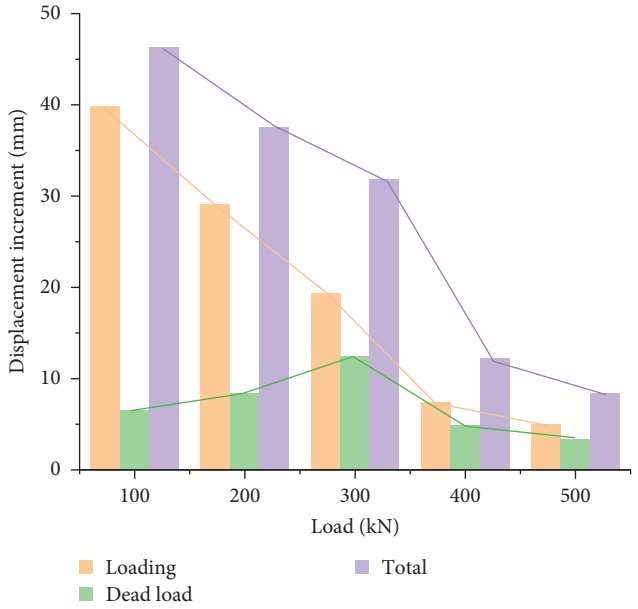

Figure 5: Displacement increment and distribution under initial saturated state.

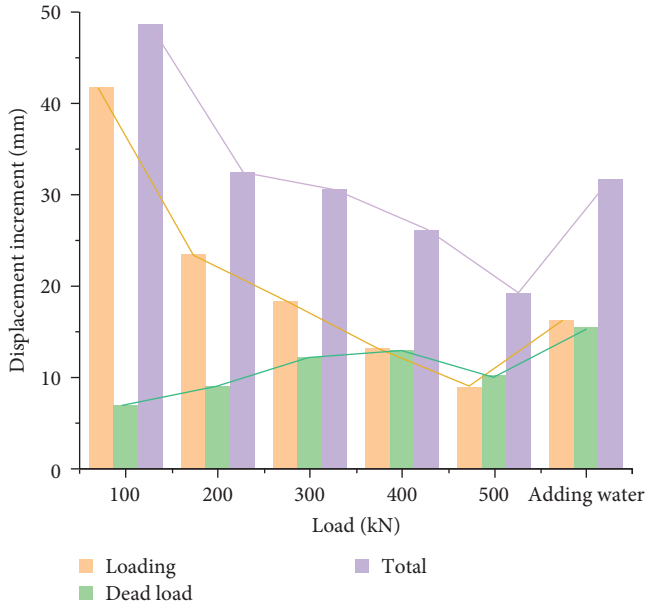

Figure 6: Displacement increment and distribution in later immersion state.

As depicted in Figure 4, the compressive deformation of broken rock exhibits a stepwise pattern, with decreasing step height as the axial load increases. At a pressure of 500 kN, the axial deformation difference of broken rock attains its minimum value. However, during the water injection stage, which lasts for only about 10 min, the axial deformation difference of broken rock exceeds that of the loading stages of 400 and 500 kN under the same load, suggesting that water significantly accelerates the compression deformation of broken rock. Given the evident changes in the water environment in the goaf, the stable deformation of loose rock blocks in the goaf may undergo deformation mutation, thereby leading to surface movement and destruction.

5. Deformation Law of Loose Rock Blocks in Different Water State

Figure 5 illustrates that in the initial state of full saturation, there is a decrease in both total deformation and deformation during the loading stage as the load gradient increases. In contrast, the deformation during the dead load stage initially increases and then decreases with increasing load gradient. The maximum deformation during the dead load stage occurs at a load gradient of 300 kN. Although the difference between them gradually diminishes, the deformation during the loading stage consistently exceeds that of the dead load stage for each load gradient.

Figure 6 illustrates that in the later immersion state, the total deformation and deformation in the loading stage decrease as the load gradient increases. The deformation in the water-adding stage shows an abrupt change. The deformation of the dead load stage initially increases and then decreases with increasing load gradient, with the maximum deformation observed at a load gradient of 400 kN. Notably, the deformation of the dead load stage increases significantly after water addition. Furthermore, after the load gradient reaches 500 kN, the deformation of the dead load stage exceeds that of the loading stage.

As shown in Figure 7, in the initial saturated state, the ratio of deformation in the loading stage to the total deformation decreases from 86% to 59% for each load gradient. In the later immersion state, the ratio of deformation in the loading stage to the total deformation decreased from 86% to 47% for each load gradient. The initial saturated state is more conducive to the deformation of the loading stage than the later soaking state.

As shown in Figure 8, in the initial saturated state, for all load gradients, the ratio of deformation in the loading stage to the total deformation is 74%, and the ratio of deformation in the dead load stage to the total deformation is 26%. In the later immersion state, for all load gradients, the ratio of deformation in the loading stage to the total deformation is 67.3%, and the ratio of deformation in the dead load stage to the total deformation is 32.7%. It can also be proved that the initial saturated state is more conducive to the deformation of the loading stage than the later soaking state, which is conducive to reducing the residual deformation and is conducive to the stability of the filling stope.

6. Deformation Mechanism of Loose Rock Blocks in Different Water State

In order to discuss the deformation mechanism of loose rock blocks, granulated the loose rock blocks to study the contact mechanism of particles, loose rock blocks support the whole structure system and form direct contact between adjacent loose rock blocks.

In natural state, it is assumed that there are n contacts between the particles j and other particles in the loose rock

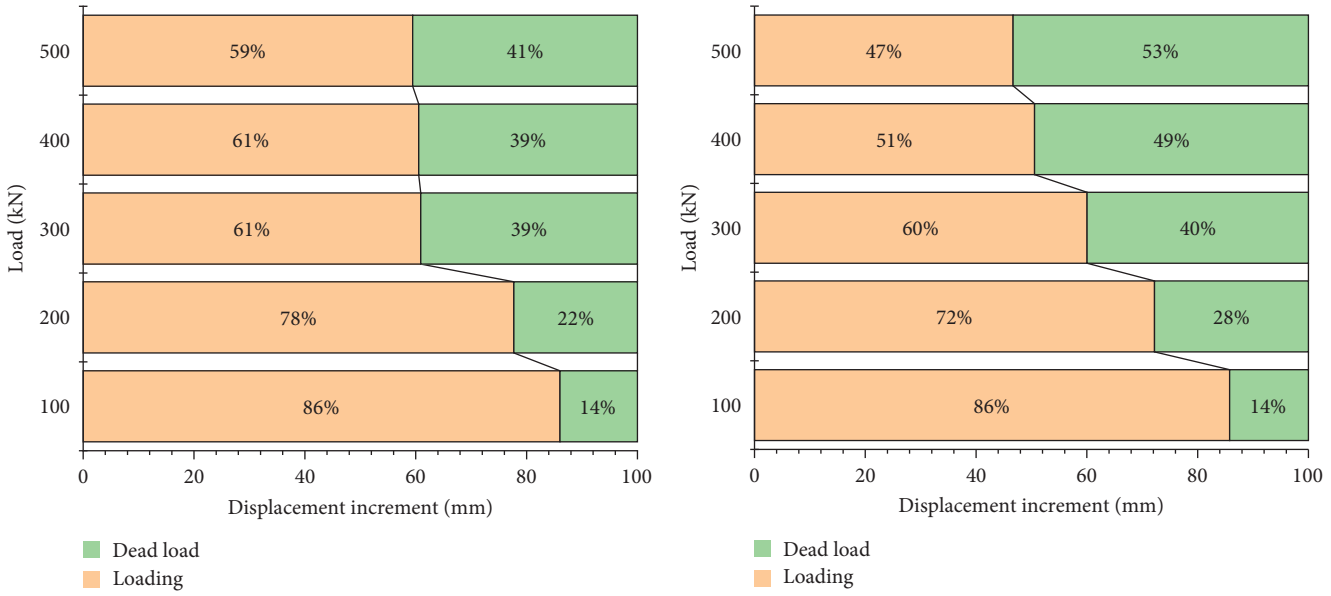

Figure 7: Proportion of deformation in different loading-dead load stages: (a) initial saturation and (b) later immersion.

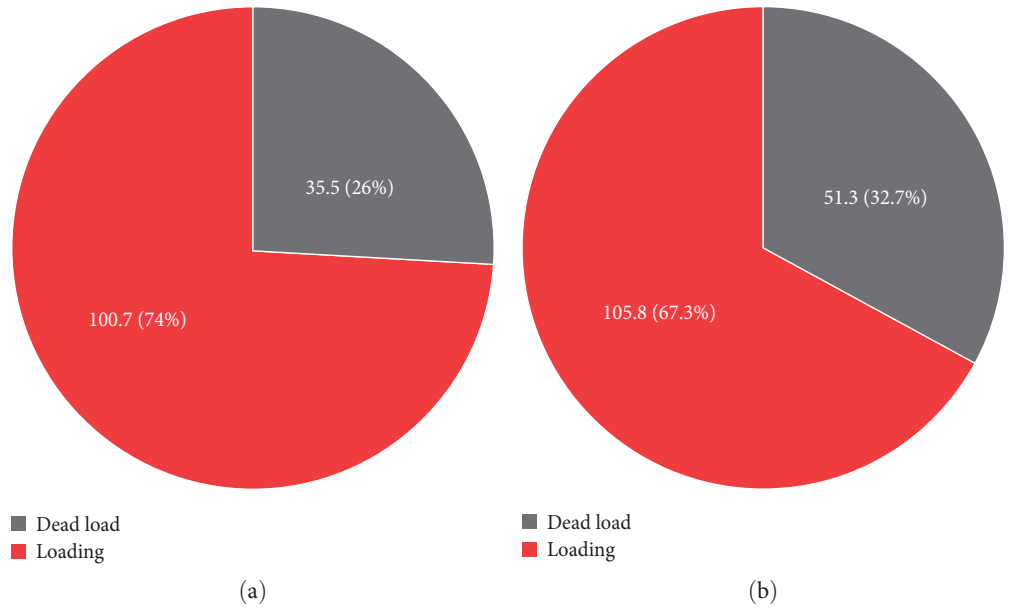

Figure 8: Proportion of deformation in loading-dead load stages: (a) initial saturation and (b) later immersion.

blocks sample. During compaction, the acting force and contact area of the ith contact is P_i, δ_i ($i = 1, 2, \ldots, n$). Taking a contact surface A of particle j as the research object, assuming that there are m contacts, there must be $m \leq n$. As shown in Figure 9, the normal stress σ_A and shear stress τ_A on contact surface A are, respectively [19]:

$$\sigma_A = \sum_{i=1}^{m} \sigma_i = \sum_{i=1}^{m} \frac{P_i}{\delta_i} \cos \alpha_i, \tag{4}$$

$$\tau_A = \sum_{i=1}^{m} \tau_i = \sum_{i=1}^{m} \frac{P_i}{\delta_i} \sin \alpha_i, \tag{5}$$

where α_i is the angle between the normal of the contact surface and the force.

In general, the compressive stress formed in the direction of total normal stress is less than the damage strength σ_s of the loose rock blocks particles, so there is no extruding and crushing between the particles. However, on the local soft

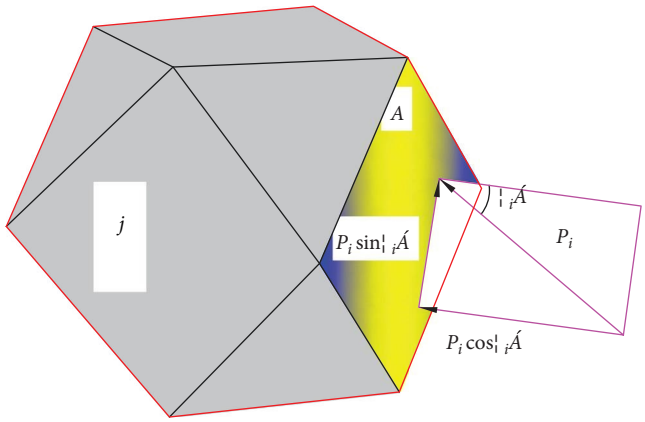

FIGURE 9: Contact between particle j and one of the other particles on an interface A.

interface or edges of the gangue particles, the damage strength σ_{sm} is often less than the corresponding contact extrusion stress σ_{im}, in which K granular weak interface will be crushed and refined by extrusion, that is to say:

$$\sigma_{im}^{k} \geq \sigma_{sm}^{k} \quad (k = 1, 2, \ldots, K). \tag{6}$$

Macroscopically, the edges and corners of the loose rock blocks and the weak interface will cause deformation caused by crushing, and the total ε_1 of the deformation will be as follows:

$$\varepsilon_1 = \sum_{k=1}^{K} \int \left(\sigma_{im}^{k} - \sigma_{sm}^{k}\right) d\zeta_k, \tag{7}$$

where ζ_k is the compression compliance, which is equal to the ratio of the strain to the compressive stress.

In addition, in Equation (4), the shear stress forms a tangential stress τ_k on the particle breakage surface, and since the contact area is small, the shear stress is approximated to be uniformly distributed, and the moment T_k on the gravity center of the particle j on the kth contact surface is given as follows:

$$T_k = \tau_k \gamma_k \sigma_k, \tag{8}$$

where r_k is the moment radius from the contact surface to the gravity center of the particle.

The sum of all shear stress torque vectors through a local coordinate (ξ–η plane) of the gravity center of the particle is given as follows:

$$T_{m\xi} = \sum_{k=1}^{K} T_k \xi_k = \sum_{k=1}^{K} P_k \sin \alpha_k \gamma_k \xi, \tag{9}$$

$$T_{m\eta} = \sum_{k=1}^{K} T_k \eta_k = \sum_{k=1}^{K} P_k \sin \alpha_k \gamma_k \eta, \tag{10}$$

where ξ_k, η_k are local coordinate projection coefficients, which are equal to the ratio of projection value and original value of shear stress on plane ξ and η, respectively.

Generally, the two moments are not zero, so the crushed particles under the action of torque produce a slight rotation or slip, which always moves toward the weak space that can move, and then acts as a filling gap. The strain ε_2 is given as follows:

$$\varepsilon_2 = \sum_{k=1}^{K} \int T_k \left(\xi_k d\theta_{\xi}^{(k)} + \eta_k d\theta_{\eta}^{(k)}\right), \tag{11}$$

where θ_ξ, θ_η is shear compliance, equal to the ratio of strain to shear stress.

It can be seen from the order of magnitude of strain value that $\varepsilon_2 > \varepsilon_1$, so the deformation of loose rock blocks caused by sliding filling gap is greater than that caused by soft interface crushing of loose rock blocks, that is, in natural state, the deformation of loose rock blocks caused by sliding filling gap is the main cause of deformation. At the end of the compression test of loose rock blocks under natural condition, the results showed that the number of loose rock blocks smaller than that of 10 mm increased the most, and the loose rock blocks of 10–60 mm decreased to some extent, which could prove the conclusion.

Particle sliding needs to overcome the friction caused by contact. From a mesoscopic point of view, the skeleton particle is not smooth in smaller scale, and its maximum static friction coefficient is related to the actual contact area. According to the theory of Archard et al. [20], it is known that μs (maximum static friction coefficient) is positively correlated with s (actual contact area), F (normal load of actual contact area) in mesoscopic friction contact of skeleton particles. When F increases, the s and μs of the skeleton particles will increase, resulting in a decreasing trend of loading deformation with the increase of load gradient.

In addition, with the increase of residence time, the maximum static friction force of the object will also increase [21]. Generally speaking, when the normal force is constant, the maximum static friction force increases with the increase of residence time. This can explain the logarithmic increase of dead load deformation, it can also explain that the sum deformation of loading stage and dead load stage decreases with the increase of load gradient.

Additionally, the influence of water on the mesostructure of unconsolidated rock blocks can affect their deformation mechanism. The filling effect of water between particles can increase their compaction and decrease the porosity, resulting in an increase in sliding and crushing deformation, and a decrease in particle rotation and deformation. Moreover, the water content can also affect the distribution and size of the pore spaces in the rock blocks, leading to an enlargement of the pores and a reduction of capillary forces, ultimately weakening the structural strength of the rock blocks.

In summary, the deformation behavior of unconsolidated rock blocks under varying water content conditions is a complex process influenced by the weakening effect of water on the effective contact stress and strength between particles, modifications in the mesostructure of the rock blocks, and changes in the distribution and size of pore spaces.

7. Conclusions

(1) In the loading stage of the initial saturated gradient loading test, a stepwise displacement increment trend was observed, characterized by a gradual reduction in the magnitude of each step. During the constant load stage, the displacement exhibited logarithmic growth, with the displacement increment showing an initial increase followed by a decrease. These stage characteristics were also observed in the later immersion gradient loading test, albeit with a notable difference in the initial saturated dead load stage, where a small step growth phenomenon and displacement rebound were observed. Furthermore, a sudden increase in displacement was noted during the later immersion water stage.

(2) The initial saturation of loose rock blocks weakens the strength and interparticle friction, leading to high deformation in the loading stage. However, the constant load stage shows a decreasing compressive deformation under the same load gradient. The later immersion stage is characterized by water acting as a lubricant, facilitating particle position adjustment, and as a carrier of broken particles, promoting small particle sliding, filling of gaps, and accelerating deformation of stable loose rock blocks. The later immersion stage exhibits a sudden increase in displacement, likely due to accelerated deformation caused by the water-induced particle sliding and gap filling. Furthermore, the initial saturation stage displays a distinct phenomenon of small step growth and displacement rebound in the dead load stage.

(3) The macroscopic strain of loose rock blocks is mainly controlled by particle porosity and particle friction coefficient. In order to optimize the macroscopic compaction mechanical properties of gangue filling, it is necessary to consider both the macro- and micro-mechanisms of loose rock blocks. To reduce porosity, precompaction and presoaking of loose rock blocks are effective measures. To increase the friction performance of gangue filling, cheap and readily available materials such as sand or fly ash can be added. Moreover, a small amount of slurry can be added to fill the gap between the loose rock blocks and increase their friction performance. These measures can effectively improve the macroscopic compaction mechanical properties of gangue filling.

Data Availability

All the data in this paper are available from the corresponding author upon request.

Conflicts of Interest

The authors declare that they have no conflicts of interest.

Authors' Contributions

All the authors contributed to publishing this paper. B.Z. and C.W. conceived the main idea of the paper; J.L. contributed to the theoretical analysis; Y.Z. and Z.Z. analyzed the data; C.W. and Y.G. wrote the paper; Q.Z. and D.K. modified the figures.

Acknowledgments

We are very grateful the financial supports from the Taishan Scholar Talent Team Support Plan for Advantaged & Unique Discipline Areas, Project No. ZR2022ME165 supported by Shandong Provincial Natural Foundation, and Science and Technology Project of Liaocheng University (nos. 318012014 and 318011901).

References

[1] C. Wang, Y. Lu, Y. Li, B. Zhang, and Y. Liang, "Deformation process and prediction of filling gangue: a case study in China," *Geomechanics and Engineering*, vol. 18, no. 4, pp. 417–426, 2019.

[2] H. Yan, J. Zhang, S. Zhang, and N. Zhou, "Physical modeling of the controlled shaft deformation law during the solid backfill mining of ultra-close coal seams," *Bulletin of Engineering Geology and the Environment*, vol. 78, pp. 3741–3754, 2019.

[3] B. Li, H. Yan, J. Zhang, and N. Zhou, "Compaction property prediction of mixed gangue backfill materials using hybrid intelligence models: a new approach," *Construction and Building Materials*, vol. 247, Article ID 118633, 2020.

[4] C. Wang, B. Shen, J. Chen et al., "Compression characteristics of filling gangue and simulation of mining with gangue backfilling: an experimental investigation," *Geomechanics and Engineering*, vol. 20, no. 6, pp. 485–495, 2020.

[5] Q. Zhang, Z. Wang, J. Zhang et al., "Integrated green mining technology of "coal mining-gangue washing-backfilling-strata control-system monitoring"–taking Tangshan Mine as a case study," *Environmental Science and Pollution Research*, vol. 29, pp. 5798–5811, 2022.

[6] L. Fan and S. Liu, "A conceptual model to characterize and model compaction behavior and permeability evolution of broken rock mass in coal mine gobs," *International Journal of Coal Geology*, vol. 172, pp. 60–70, 2017.

[7] F. Zhu and W. Zhang, "Scale effect on bearing capacity of shallow foundations on strain-softening clays," *Computers and Geotechnics*, vol. 135, Article ID 104182, 2021.

[8] C.-M. Hu, X.-Y. Wang, Y. Mei, Y.-L. Yuan, and S.-S. Zhang, "Compaction techniques and construction parameters of loess as filling material," *Geomechanics and Engineering*, vol. 15, no. 6, pp. 1143–1151, 2018.

[9] M. Li, A. Li, J. Zhang, Y. Huang, and J. Li, "Effects of particle sizes on compressive deformation and particle breakage of gangue used for coal mine goaf backfill," *Powder Technology*, vol. 360, pp. 493–502, 2020.

[10] P. Huang, J. Zhang, X. Yan, A. J. S. Spearing, M. Li, and S. Liu, "Deformation response of roof in solid backfilling coal mining based on viscoelastic properties of waste gangue," *International Journal of Mining Science and Technology*, vol. 31, no. 2, pp. 279–289, 2021.

[11] G. Wang, M. Wu, R. Wang, H. Xu, and X. Song, "Height of the mining-induced fractured zone above a coal face," *Engineering Geology*, vol. 216, pp. 140–152, 2017.

[12] J. Xie and J. Xu, "The corresponding relationship between the change of goaf pressure and the key stratum breaking," *Journal of Geophysics and Engineering*, vol. 16, no. 5, pp. 913–925, 2019.
[13] J. Li, Y. Huang, M. Qiao et al., "Effects of water soaked height on the deformation and crushing characteristics of loose gangue backfill material in solid backfill coal mining," *Processes*, vol. 6, no. 6, Article ID 64, 2018.
[14] Y. Lu, N. Jiang, W. Lu et al., "Experimental study on deformation characteristics of gangue backfill zone under the condition of natural water in deep mines," *Sustainability*, vol. 14, no. 23, Article ID 15517, 2022.
[15] Z. Ma, T. Lan, Y. Pan, J. Ma, and F. Zhu, "Experimental study on pore variation law during creep process of saturated fractured mudstone," *Chinese Journal of Rock Mechanics and Engineering*, pp. 1447–1454, 2009.
[16] Z. Ma, G. Guo, R. Chen, and X. Mao, "An experimental study on the compaction of water-saturated over-broken rock," *Chinese Journal of Rock Mechanics and Engineering*, vol. 7, pp. 1139–1144, 2005.
[17] X. Chen, C. Su, X. Tang, and W. Guo, "Experimental study on the effect of saturated water on the compaction characteristics of crushed rock on coal seam roof," *Chinese Journal of Rock Mechanics and Engineering*, vol. 33, pp. 3318–3326, 2014.
[18] C. Wang, Y. Lu, G. Hao, B. Cui, and Z. Zhao, "Simulated test on compression deformation characteristics and mechanism of fractured rock in mined out area," *Geotechnical and Geological Engineering*, vol. 36, pp. 2809–2821, 2018.
[19] J. Zhang, H. Wang, S. Chen, and Y. Li, "Compressive deformation characteristics of crushed rock with large particle size," *Journal of China Coal Society*, vol. 43, pp. 1000–1007, 2018.
[20] J. F. Archard, "Elastic deformation and the laws of friction," in *Proceedings of the Royal Society of London. Series A, Mathematical and Physical Sciences*, vol. 243, 1957.
[21] S. Kato, N. Sato, and T. Matsubayashi, "Some considerations on characteristics of static friction of machine tool slideway," *Journal of Lubrication Technology*, vol. 94, no. 3, pp. 234–247, 1972.